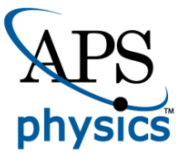

Efficient Excitation of High-Frequency Exchange-Dominated Spin Waves in Periodic Ferromagnetic Structures

Aryan Navabi, Cai Chen, Anthony Barra, Mohsen Yazdani, Guoqiang Yu, Mohammad Montazeri, Mohammed Aldosary, Junxue Li, Kin Wong, Qi Hu, Jing Shi, Gregory P. Carman, Abdon E. Sepulveda, Pedram Khalili Amiri, and Kang L. Wang

Phys. Rev. Applied **7**, 034027 — Published 28 March 2017

DOI: 10.1103/PhysRevApplied.7.034027

Efficient excitation of high-frequency exchange-dominated spin-waves in periodic ferromagnetic structures

Aryan Navabi[1], Cai Chen[2], Anthony Barra[2], Mohsen Yazdani[1], Guoqiang Yu[1], Mohammad Montazeri[1], Mohammed Aldosary[3], Junxue Li[3], Kin Wong[1], Qi Hu[1], Jing Shi[3], Gregory P. Carman[2], Abdon E. Sepulveda[2], Pedram Khalili Amiri[1], Kang L. Wang[1]

[1]Department of Electrical Engineering, University of California, Los Angeles, California 90095, USA

[2]Mechanical and Aerospace Engineering Department, University of California, Los Angeles, California 90095, USA

[3]Department of Physics and Astronomy, University of California, Riverside, CA 92521, USA

Spin waves are of great interest as an emerging solution for computing beyond the limitations of scaled transistor technology. In such applications, the frequency of the spin waves is important as it affects the overall frequency performance of the resulting devices. In conventional ferromagnetic thin films, the magnetization dynamics in ferromagnetic resonance (FMR) and spin-waves are limited by the saturation magnetization of the ferromagnetic (FM) material and the external bias field. High-frequency applications would require high external magnetic fields which limit the practicality in a realistic device. One solution is to couple microwave excitations to perpendicular standing spin-waves (PSSWs) which can enable higher oscillation frequencies. However, efficient coupling to these modes remains a challenge since it requires an excitation that is non-uniform across the FM material thickness and current methods have proven to be inefficient, resulting in weak excitations. Here, we show that by creating periodic undulations in a 100 nm thick $Co_{40}Fe_{40}B_{20}$ layer, high-frequency PSSWs (>20 GHz) can be efficiently excited using micrometer sized transducers at bias fields below 100 Oe which absorb nearly 10% of the input RF power. Efficient excitation of such spin-waves at low fields may enable high-

frequency spintronic applications using exchange-dominated magnetic oscillations using very low external magnetic fields and, with design optimizations, can bring about new possibilities in the field.

Corresponding author email: aryan.n@ieee.org, wang@ee.ucla.edu

I. INTRODUCTION

Spin-waves in FM materials have many applications such as carrying spin currents [1,2], in logic devices [3–5], and information propagating busses [6] among others [7]. Spin-waves in FM materials are typically excited using a DC bias, H_{bias}, and an RF, h_{rf}, magnetic field, with h_{rf} having a component perpendicular to H_{bias}. The excited spin-wave mode is determined by the angle between H_{bias} and the spin-wave propagation direction, as well as their orientation with respect to the FM layer [8]. These modes differ in their dispersion relation, i.e. the relation between the spin-wave oscillation frequency and its wavenumber k for a given H_{bias} in an FM material of saturation magnetization M_S [8]. Of particular interest are magnetostatic surface spin-waves (MSSWs) due to their surface nature and comparatively higher frequency and group velocity. However, the frequency is still limited by the M_S value of the FM material and for higher frequencies, higher magnetic fields are required which limits the realization of RF applications using spin-waves, e.g. bias fields of above 1000 Oe for frequencies above 12 GHz for CoFeB. It has been shown that by separating two FM layers with a thin non-magnetic layer, a resonant frequency of 27 GHz at a bias field of 60 Oe can be achieved [9], however this method requires sub-nanometer accuracy of thin film deposition.

Another spin-wave mode that has been less utilized is PSSW [10]. Compared to MSSWs, PSSWs can be excited at higher frequencies. This is due to the fact that PSSWs are confined by the FM material and can have large wavenumbers and thus highly exchange-dominated. Thus, PSSWs have mainly been used to study and measure exchange interactions [11,12], exchange stiffness [13–15], and damping [16] in FM materials. Recently, PSSWs have been used in switching field reduction of highly coercive magnets [17]. However, excitation of such spin-waves requires a non-uniform dynamic field across the thickness of the

FM layer [10] such as using high power lasers [2,18,19]. Other methods include using a microstrip [16,20], but these have proven to be highly inefficient since there is little coupling between the RF magnetic field created by the microstrip and the PSSW modes [10,20,21]. PSSW can also be excited by an out of plane magnetic field, however, in the case of FM materials such as Permalloy or CoFeB, they require bias fields above 10^4 Oe [16] which significantly limits their practical applications. Efficient excitation of such exchange-dominated spin-wave modes could potentially have implications for novel high-frequency spintronic application.

Here, we demonstrate efficient excitation of high-frequency PSSW resonances by creating a periodic undulation in a 100 nm thick CoFeB layer using micrometer scale coplanar waveguides (CPWs) as transducers. Spin-waves were excited at two resonant frequencies for low bias fields, with the lower frequency at the MSSW mode and the higher one at PSSW mode. High-frequency oscillations above 20 GHz were excited at fields even below 100 Oe. To achieve the same oscillation frequency using MSSW, a bias field above 2500 Oe is required. More importantly, the periodic undulation results in efficient coupling of microwave excitations to these non-uniform modes. Same measurements were performed on flat and undulating YIG structures and the same effects were also observed proving that the undulation of the FM layer leads to the observation of the second higher frequency mode. A finite difference time domain (FDTD) Micromagnetic simulation was used to confirm the excitation of PSSW modes. Good agreement was found between both experimentally and simulated observed absorption peaks for CoFeB and YIG samples. The simulation results also provided an insight into the dynamics of these standing spin-waves.

II. EXPERIMENTAL DETAILS

We created a one dimensional undulating SiO_2 layer on a lightly doped Si substrate. The steps of making such undulating substrates is presented in the supplementary materials, section I [22] [23]. The pattern will be transferred to any material deposited on top of such substrate and no further patterning is required. 100 nm thick layers of CoFeB and YIG where deposited separately using a high-vacuum magnetron

sputtering system and by pulsed laser deposition, respectively. Cross sectional SEM image of the 100 nm CoFeB film deposited on the undulating SiO_2 substrate is shown in Fig. 1(a).

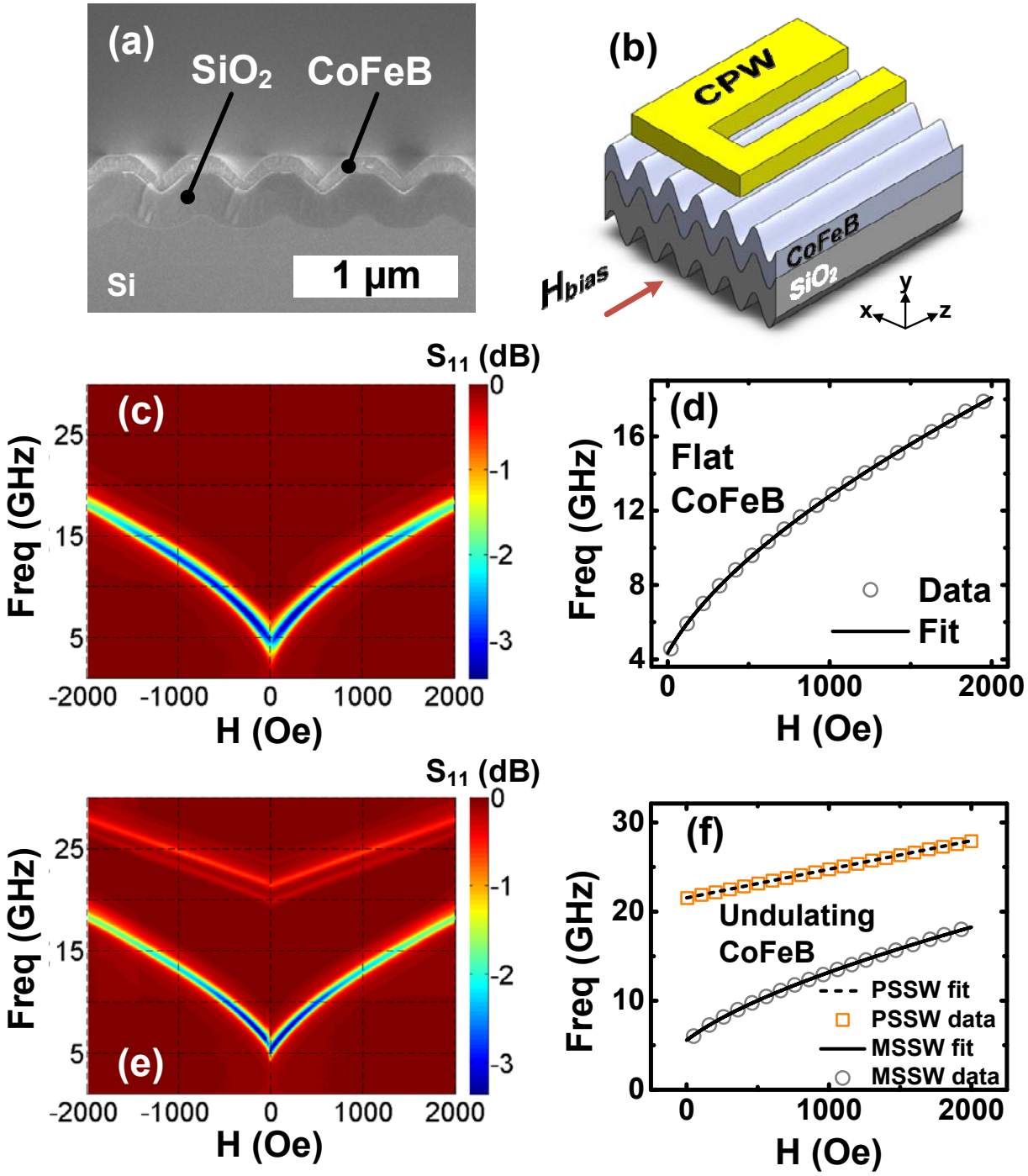

Figure 1. S_{11} parameters of measured flat and undulating CoFeB layers. a. Cross sectional SEM image shows that the 100 nm thick CoFeB layer deposited on the undulating substrate inherits the

topography of the substrate. b. Schematic of the spin-wave device. An external magnetic field, H_{bias}, with a dynamic magnetic field originating from an RF current in the CPW is used to excite spin waves. c. Measured S_{11} parameter of 100 nm thick flat CoFeB layer. d. Measured data for the MSSW mode (circles) along with fitted curve (solid line) using the MSSW dispersion relation (Eq. 1). e. Measured S_{11} parameter of 100 nm thick undulating CoFeB layer with topography shown in Fig. 1(f). f. Measured data for the MSSW and PSSW modes, circles and squares, respectively, along with fitted curves using the MSSW dispersion relation (Eq. 1), bottom solid line, and PSSW dispersion relation (Eq. 2), top dashed line.

After the deposition, the CoFeB layer was etched into an area of 500 μm by 100 μm. A 500 nm thick SiO_2 was deposited and used as an insulation between the transducers and CoFeB layer. Flat FM layer samples were also prepared for control experiments by using the non-patterned areas of the samples. Next, CPW structures were deposited and used as transducers to excite spin-waves. A copper layer 1.2 μm thick with a 90 nm thick chrome layer as adhesion was used as CPW. The width of the signal line (S) is 8 μm. The ground line (G) is twice as wide as the signal line of each sample. The separation between the ground and signal lines is equal to the width of the signal line. Prior to measurements, a vector network analyzer (VNA) was calibrated up to 30 GHz using a standard calibration kit. The schematic of the spin-wave device is shown in Fig. 1(b). Magneto static surface waves (MSSW) were excited and S-parameters were measured by means of VNA-ferromagnetic resonance, and by aligning H_{bias} along the z direction [see Fig. 1(b)] [24,25]. H_{bias} was swept from -2000 to 2000 Oe and S-parameters were measured and recorded. Background electromagnetic coupling was eliminated by comparing S-parameters at resonant and non-resonant conditions [25].

III. RESULTS AND DISCUSSION

A. CoFeB

We first analyzed spin-waves in our flat CoFeB control sample. Fig. 1(c) shows the S_{11} parameter measured after removing the background electromagnetic coupling. The color map represents the

magnitude of the power absorbed by the spin-waves excited in the FM layer under the signal line. The curved line observed in the S-parameters is the MSSW mode, also called the Damon-Eshbach mode, and the dispersion relation is given by [8]

$$(2\pi f)^2 = \left(\omega_H + \frac{\omega_M}{2}\right)^2 - \left(\frac{\omega_M}{2}\right)^2 \exp(-2kd) \qquad \text{(Eq. 1)}$$

, where ω_H is given by γH_{bias} and ω_M is given by $\gamma\mu_0 M_S$ with M_S in units of $A \cdot m^{-1}$ and μ_0 the permeability of free space equal to $4\pi x10^{-7}$ H/m, with d as the thickness of the CoFeB layer; in this case, 100 nm. γ is the gyromagnetic ratio which is given by $g_e m_B/\hbar$, where g_e is the Landé g-factor, m_B is the Bohr magneton, and $\hbar$ is the reduced plank's constant. The curve in Fig. 1(c) was used and fitted to the above equation [Fig. 1(d)]. Values of 28 $GHz \cdot T^{-1}$ for γ and 1408 $^{emu}/_{cc}$ for M_S were determined which are typical values for CoFeB [15]. Using Eq.1 we estimated the wavenumber k to be $1.47x10^5$ m^{-1} which is close to values determined by numerical methods [16,26,27]. Next we performed the same measurement process with our undulating CoFeB sample. Fig 1(e) shows the S_{11} parameter where a second resonance was observed at higher frequencies. By fitting the second resonance with the dispersion relation for PSSW mode [Fig. 1(f)] , given by [2,10,28]

$$2\pi f = \gamma \left[\begin{array}{l} \left(H + H_K + \frac{2A}{M_S} k_{\parallel}^2 + \frac{2A}{M_S}\left(\frac{p\pi}{d}\right)^2 \right) \times \\ \left(H + H_K + \left[\frac{2A}{M_S} + H\left(\frac{4\pi M_S/H}{p\pi/d}\right)^2 \right] k_{\parallel}^2 + \frac{2A}{M_S}\left(\frac{p\pi}{d}\right)^2 + 4\pi M_S F_p \right) \end{array} \right]^{1/2} \qquad \text{(Eq. 2)}$$

, we determined that the second mode is indeed PSSW and thus a consequence of non-uniform excitation of magnons across the FM layer thickness. In the equation above, H_k is the field created by the shape anisotropy, which we found to be negligible in magnitude, A is the exchange stiffness in units of $J \cdot m^{-1}$ and was estimated to have a value of approximately 28.4 $pJ \cdot m^{-1}$ which is similar to other values determined for CoFeB films [15]. $k_{\parallel}$ is the in-plane wavenumber, and p is the PSSW mode number that

corresponds to the number of nodes in the mode profile across the thickness of the CoFeB layer, and F_p is a constant that depends on the pinning parameter [28,29]. The total wavenumber k is given by $\sqrt{k_{||}^2 + \left({}^{p\pi}/_{d}\right)^2}$. By fitting the first mode (MSSW) in Fig 1.e with Eq. 1 and using the values of γ and M_S derived from measuring the control flat CoFeB sample, k was estimated to be $2.56\text{x}10^5$ m^{-1}. For the PSSW mode, the value of k for the MSSW mode was used as $k_{||}$. However, as will be shown, $k_{||}$ is much smaller than the out-of-plane wavenumber and does not change the fitting significantly. The same values of M_S and γ form MSSW mode were also used for the PSSW. We determined that the out of plane wavenumber, ${}^{p\pi}/_{d}$, is equal to $9.94\text{x}10^7$ m^{-1}. Using the cross section SEM image shown in Fig 1.a, we estimated the thickness of the FM layer on the sloped regions to be around 70 nm. This means that p is just over 2.2. The second fitting parameter in the PSSW mode is Fp, the pinning parameter, which was estimated to be 0.6. Determining the exact values of such parameters is a long standing problem [28], therefore we performed simulation of our structure to examine the validity of some of these parameters and the results are presented in the later sections.

B. YIG

In addition to a flat CoFeB as a control experiment and to further analyze and confirm the effect of the undulating substrate on FM materials, we performed the same measurements and analysis on a 100 nm YIG film deposited on flat and undulating substrates. Preparation of the YIG samples on the SiO_2 substrates can be found in section II of the supplementary materials [22]. Fig. 2(a) shows the measured S_{11} parameter for the flat YIG sample. For our YIG samples, the width of the signal and ground lines are 24 and 48 μm, respectively. The gap between the signal and ground line is equal to the width of the signal line. We performed the same fitting process for the S_{11} parameter (Fig. 2(b)). γ, M_S, and the wavenumber obtained for the flat YIG sample are 29.9 $GHz \cdot T^{-1}$, 87.5 ${}^{emu}/_{cc}$, and $5\text{x}10^5$ m^{-1}, respectively. The quality of the YIG is not as good as those deposited on gadolinium gallium garnet

(GGG) substrates which could be the reason behind the low value of M_S [27]. The M_S value was also confirmed by SQUID measurements. Fig. 2(c) shows the S_{11} parameter for the undulating YIG sample.

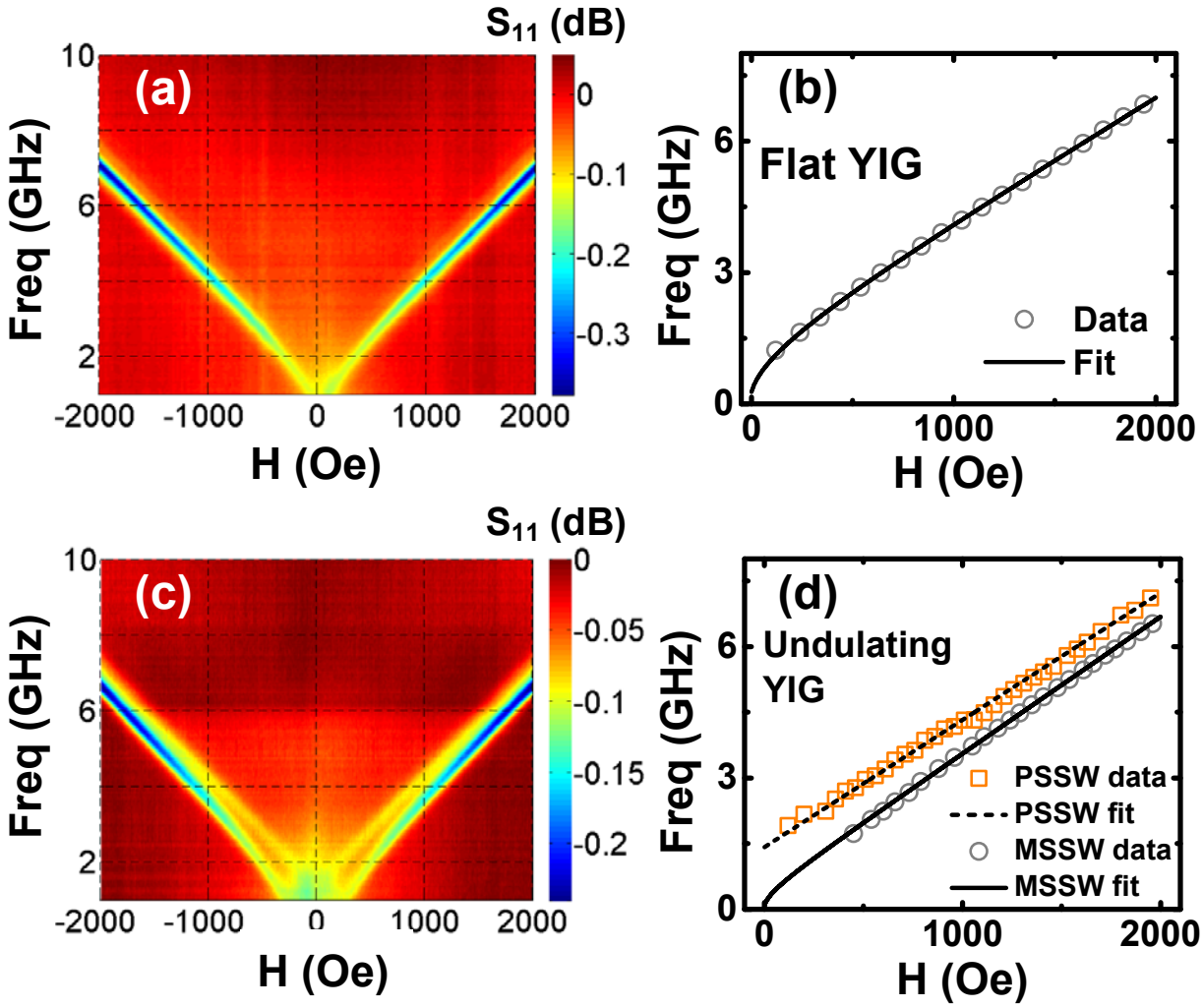

Figure 2. S_{11} parameters of measured flat and undulating YIG layers. a. Measured S_{11} parameter of 100 nm thick flat YIG layer. b. Measured data for the MSSW mode (circles) along with fitted curve (solid line) using the MSSW dispersion relation (Eq. 1). c. Measured S_{11} parameter of 100 nm thick undulating YIG layer with topography shown in Fig. 1(f). d. Measured data for the MSSW and PSSW modes, circles and squares, respectively, along with fitted curves using the MSSW dispersion relation (Eq. 1), bottom solid line, and PSSW dispersion relation (Eq. 2), top dashed line.

Compared to the flat control sample, a second mode less than a GHz above the main mode was observed. The first mode was fitted with the MSSW dispersion relation (Eq. 1) and a smaller M_S value of 71.6

$emu/_{cc}$ was obtained which was also confirmed by SQUID measurements. The difference in saturation magnetization between flat and undulating YIG could be due to the strong dependence of YIG quality on substrate. Not only the oxide substrate is not suitable for high quality YIG, the undulating substrate could also affect magnetic properties of the grown YIG film [30]. The second mode was also fitted to the PSSW dispersion relation (Fig. 2(d)) and by using the same analysis that was performed with undulating CoFeB layer, an out-of-plane wavenumber of 9.98 E7 m^{-1} and an exchange stiffness of $3.7\text{x}10^{-2}\ pJ \cdot m^{-1}$ was obtained. The exchange stiffness for the YIG used in these experiments is 2 orders of magnitude smaller than YIG grown on GGG [14]. This could be again due to the choice of substrate, undulating SiO_2, which can alter the material properties of the deposited YIG.

IV. SIMULATION AND RESULTS

A. Micromagnetic Simulation Setup

To confirm the dominance of the PSSW mode's contribution to the undulating FM's resonant behavior, an FDTD micromagnetic simulation was created using MuMax3 [32]. The simulated magnetic state was time evolved in accordance with the Landau-Lifshitz-Gilbert equation (see supplementary materials, section III) [22] [31], taking into account the Zeeman, exchange, and demagnetizing effective fields.

To model the undulating FM geometry (Fig. 3(a)), a 50 nm wide cross-sectional slice of one period was approximated by a trapezoidal arch (Fig. 3(b)). The space in this element was discretized using 2×2×2 nm^3 cuboidal finite difference cells, whose sizes were picked because they are smaller than the exchange lengths of CoFeB and YIG [14,15,32]. To capture the effects of long range coupling in large area films, periodic boundary conditions were applied on the magnetic state in the x and z-directions. These periodic conditions enforced 1) that the magnetization **m** at the two opposing boundaries (red dashed lines in Fig. 3(b)) were held equal and 2) that a number of repeated images of the magnetic state are added to the ends of the geometry when calculating the magnetostatic field. Consequently, a separate parametric study was done to find the number of periodic images that were required to ensure convergence of the dynamic micromagnetic behavior (see supplementary materials, section IV) [22]. Convergent behavior was

reached with 50 images in both ±z directions, as the model approached a large aspect ratio limit, but periodic images in ±x did not strongly affect the result since the PSSW modes of interest exist along y. Three images in both ±x directions were kept to allow any dipolar coupling between neighboring arch elements.

To probe the structure's resonant modes the following protocol was used: 1) a bias field H_{bias} was applied in the z direction to ensure a single domain configuration; then, 2) a broadband Gaussian magnetic field pulse with 50 Oe magnitude was applied in the x-direction. Details for the pulse shape can be found in supplementary materials, section IV [22]. The time-domain response of magnetization was recorded by taking the m_x, m_y, and m_z components averaged over the volume every 0.5 ps. The time response was then Fourier transformed to yield the frequency dependent susceptibility. This process was then repeated while sweeping H_{bias} from 500 to 1500 Oe in 100 Oe steps to recover the full field-frequency dependent absorption.

This protocol was used to create simulated absorption spectra for all four of the fabricated samples, which include both undulating and flat control samples, made from both CoFeB and YIG, as described in Section 1. Table 1 shows key materials parameters used in the protocol. The flat sample model geometry was 500×100×50 nm^3. The periodic conditions, the bias field, and the excitation protocols were matched with those previously mentioned.

Once the absorption spectrum was determined, additional simulations were carried on the undulating CoFeB sample. The structure was harmonically driven at both resonant frequencies for a bias field of 1000 Oe. This allowed for analysis of the time-domain magnetic responses which were plotted into x-y plane cross section animations to spatially locate the dominant standing modes which shall be discussed later in this work.

Table 2. Key materials parameters used for Micromagnetics simulations.

	CoFeB	**YIG**
$\mathbf{M_S}$ $(\boldsymbol{emu/cc})$	1408	87.5[a]

$\mathbf{A_{ex}}$ ($^{pJ}/_{m}$)	28.4	0.037
α	0.035	0.01[b]

[a]An M_s value of 71 $^{emu}/_{cc}$ was used for undulating YIG, which was based on SQUID measurements.

[b]The Gilbert damping for thin film YIG grown on SiO_2 substrate was taken to be orders of magnitude higher than that for bulk YIG based on propagating spin-wave spectroscopy.

B. Micromagnetic Simulation Results

Fig. 3(c-d) show absorption plots for a fixed bias field of 1000 Oe for flat (blue lines) and undulating (red lines) films for both CoFeB and YIG samples. The amplitudes are normalized by the maximum absorption of the corresponding flat samples. The full field-frequency dependent absorption for the flat and undulating CoFeB and YIG, shown in Fig. 3(e-h), were obtained by taking the local maxima of the normalized absorption plots for fields ranging from 500 to 1500 Oe. When contrasted with those for the flat CoFeB and YIG (Fig. 3(e) and 3(g), and the blue lines in Fig. 3(c-d)), it is clear that the dual resonances are unique to the undulating geometries. One of these modes forms at low frequencies (MSSW) and one at high frequencies (PSSW).

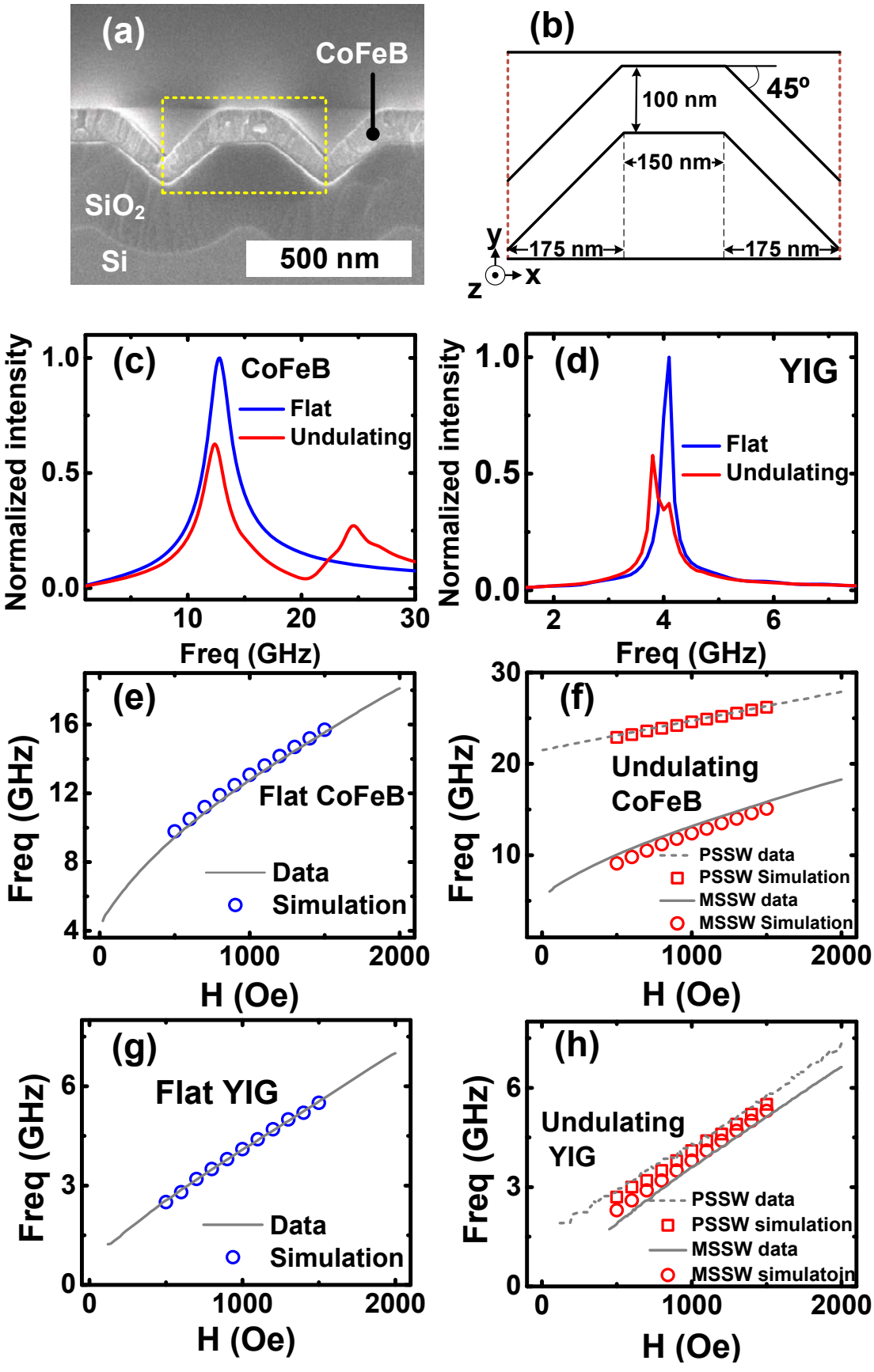
(a)
CoFeB
SiO2
Si
500 nm
(b)
100 nm
45º
150 nm
175 nm
175 nm
y
z
x
(c)
CoFeB
Flat
Undulating
Normalized intensity
Freq (GHz)
(d)
YIG
Flat
Undulating
Normalized intensity
Freq (GHz)
(e)
Flat CoFeB
Data
Simulation
Freq (GHz)
H (Oe)
(f)
Undulating
CoFeB
PSSW data
PSSW Simulation
MSSW data
MSSW Simulation
Freq (GHz)
H (Oe)
(g)
Flat YIG
Data
Simulation
Freq (GHz)
H (Oe)
(h)
Undulating
YIG
PSSW data
PSSW simulation
MSSW data
MSSW simulatoin
Freq (GHz)
H (Oe)

Figure 3. Micromagnetic model geometry and simulated S_{11} parameters for the undulating and flat CoFeB and YIG FM's. (a) SEM image detailing the as-fabricated undulating FM structure which was approximated for the model geometry. (b) The FDTD model approximation to the structure in (a), most importantly showing matching out-of-plane thickness dimensions (where the PSSWs form). (c) A comparison is made between the frequency dependent susceptibility of flat and undulating CoFeB for a z-directed 1000 Oe bias field. (d) The same comparison made in (c) for CoFeB is made for YIG. Note the comparatively smaller gap between resonances for YIG. (e) The absorption spectrum is shown for flat CoFeB. Grey lin indicate peaks in experimentally measured absorption whereas blue circle markers indicate the corresponding simulated peaks. (f) The measured (solid and dashed lines) and simulated (red circle and square markers) absorption spectrum for undulating CoFeB. (g) The comparison between experimental and simulated absorption is made for flat YIG. (h) The same comparison is made as in (f-g), but for undulating YIG.

The PSSW was mostly dominated in the structure's sloped regions which was confirmed using animations of the magnetic time response to analyze where the standing modes appear when the structure is resonantly driven. Several snap shots from the animations are shown in Fig. 4. Fig. 4(a-c) show the normalized y-component of dynamic magnetization, $\widetilde{m_y}$, for the whole structure where red is $\widetilde{m_y}$ = +1, and blue is $\widetilde{m_y}$ = -1, at 160, 180, and 200 ps, while the structure is being driven in a 1000 Oe z-directed bias field by a 50 Oe resonant 12.4 GHz uniform external field. These images show a uniform mode in the structure's sloped regions. At 24 GHz (Fig. 4(d-f)), the mode becomes non-uniform as indicated by the inset in Fig. 4(f) which shows the y-component of the magnetization in the left sloped region indicated by the black dashed line (at 171, 181, 192 ps). The inset shows two nodes in the standing spin-wave which confirms the value determined for p in the PSSW dispersion relation (Eq. 2) by fitting to the experimental data. This demonstrates that the higher frequency mode must be from non-uniform excitation across the thickness of the FM layer, which we attribute to the angle of the sloped regions.

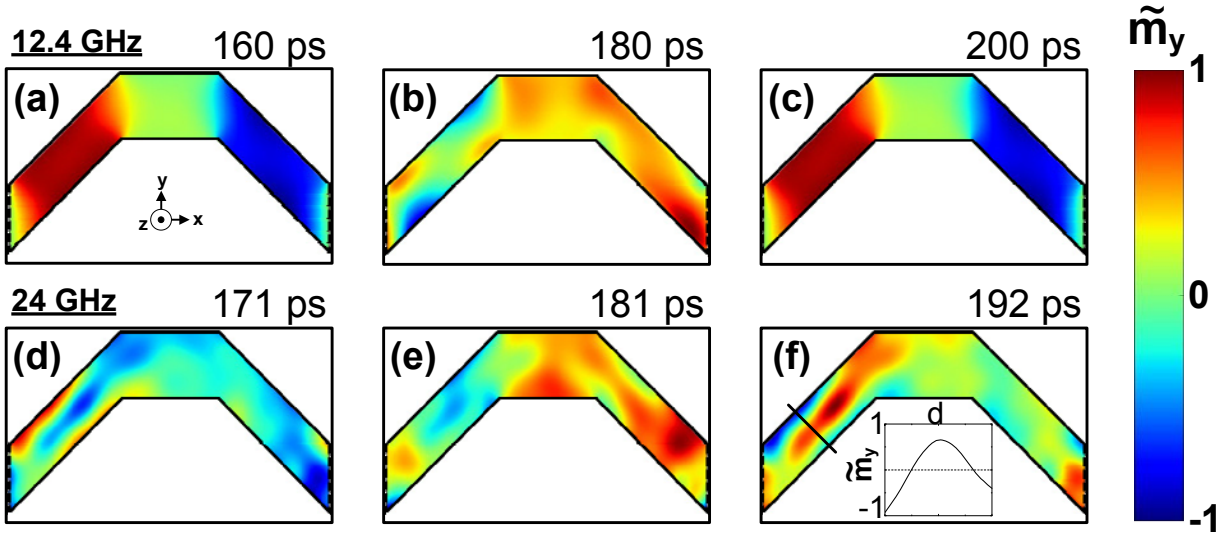

Figure 4. The m_y component is plotted structure-wide while being driven at resonant frequencies in a z-directed 1000 Oe bias field. (a-c) A uniform mode excitation is generated at 12.4 GHz in the structure's left sloped region. In (a) the left sloped region is red, indicating $\widetilde{m_y} = 1$, in (b) it averages to 0, so $\widetilde{m_y} \approx 0$, and in (c) it is red, so $\widetilde{m_y} = 1$ again. Since each sloped region has a constant color, the oscillations are in phase, and thus showing the dynamics of the fundamental mode. (d-f) The PSSW mode is excited in the left sloped region by driving it externally at 24 GHz. (d) shows a red-blue-red profile through the thickness of the left sloped region, whereas (f) shows a blue-red-blue profile. The inlay in (f) indicates that this profile (cross section at solid line) corresponds to a sinusoidally shaped PSSW mode.

Since we are reporting good agreement between simulation and experiment for all four structures (flat and undulating, for both CoFeB and YIG), we take the simulated dynamics to accurately reflect the dynamics of the fabricated structures. The simulations also support the exchange stiffness values determined by fitting the experimental data with values of A_{CoFeB}=28.4 $pJ \cdot m^{-1}$ and A_{YIG}=3.7x10^{-2} $pJ \cdot m^{-1}$.

V. DAMPING

Next we show the effect of the undulation on the damping by measuring the frequency dependence of the linewidth in these two samples. One might expect that the change in topography would have negative effects such as enhancing damping in such FM layers. However, our measurements from three different samples of both flat and undulating CoFeB layer show a reduction in the linewidth. Fig. 5 shows the measured linewidth for a flat and undulating CoFeB.

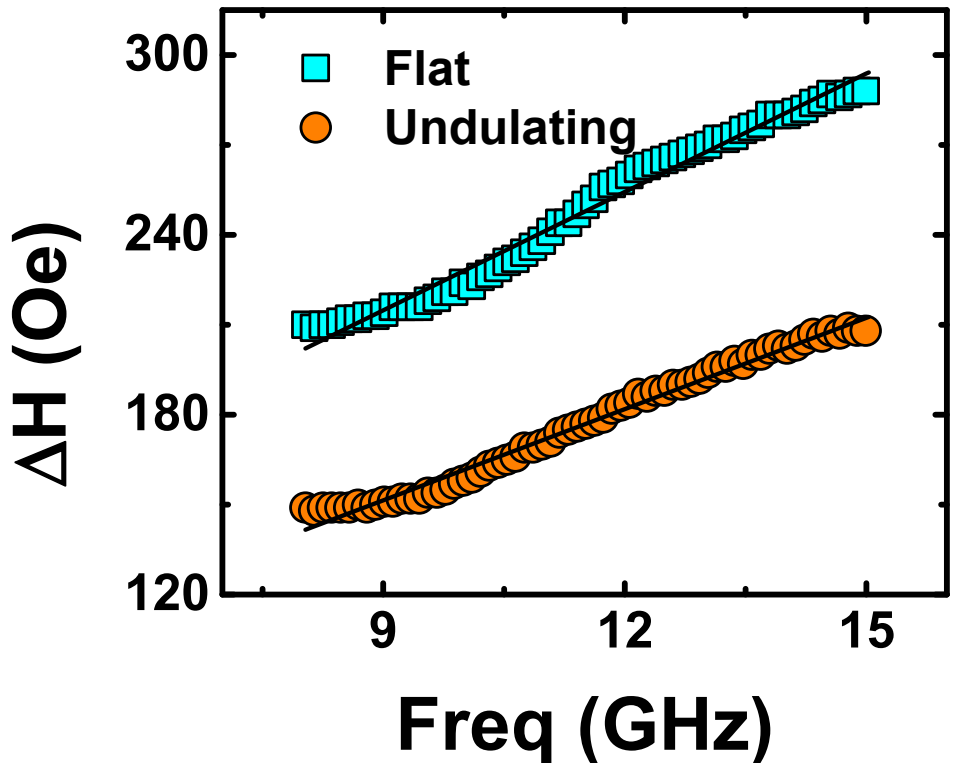

Figure 5. Frequency dependent linewidth of the flat (squares) and undulating (circles) CoFeB layer. Equation 3 was used to fit the data (solid lines). The measurements show a smaller offset, and thus a lower extrinsic damping, for undulating samples, in this case, 60.1 Oe, while for the flat sample it was determined to be 96.3 Oe. The fitted line for the undulating sample is also smaller and it corresponds to a Gilbert damping value of 0.0246, whereas the Gilbert damping for the flat sample was estimated to be 0.0319

We used the relation

$$\Delta H = \Delta H_{ext} + \frac{2}{\sqrt{3}} \frac{\alpha \omega}{\gamma} \quad \text{(Eq. 3)}$$

to determine the damping [33], where ΔH is the total linewidth in Oe and ΔH_{ext} is the linewidth caused by damping from extrinsic effects and α is the Gilbert damping, intrinsic to the FM material. ω is the oscillation frequency in radians. As shown in Fig. 5, the undulating sample has both a smaller offset and a smaller slope which correspond to a smaller extrinsic and intrinsic damping, respectively. Table 2 summarizes measurements from three samples of each kind.

Table 2. Summary of measured intrinsic and extrinsic damping from three flat and three undulating samples. Resuls show the undulating sample has a smaller intrinsic and extrinsic damping.

	Flat	**Undulating**
$\boldsymbol{\alpha}$	0.036 ± 0.019	0.024 ± 0.015
$\boldsymbol{\Delta H_{ext}\ (Oe)}$	93 ± 8	64 ± 10

We speculate the change in damping originates from the change in CoFeB film resistance. The undulation of the metallic film results in an increase in resistance which in turn decreases the eddy currents. However, a more quantitative analysis would be needed to fully understand this effect.

VI. EXCITATION EFFICIENCY

Finally, we address the excitation efficiency of the PSSW mode. Figure 5.a shows percentage of the absorbed RF power by the undulating CoFeB for bias fields of 80 and 500 Oe determined by analyzing the S_{11} data. These are cross section of figure 4.c but with the units converted from dB to percentage. The orange squares in Fig 5.b show the power absorbed at the center frequency of the PSSW mode for fields ranging from 80 Oe to 1990 Oe. The results show a maximum absorption of almost 10% by these

modes for our device structure and dimensions. This absorption can be improved by changing the device length. Hence, we define the term relative excitation efficiency as the power absorbed by the PSSW mode normalized by the power absorbed by the MSSW mode. The blue circles in Fig. 8.b show the relative excitation which ranges from 20% to just above 30%. Compared to other methods of exciting PSSW using CPWs, where these modes are observed as only minor resonances [13], the method presented here shows great promise for efficient excitation of these exchange-dominated modes. A key limiting factor in realizing practical spin-waves applications is the requirement for a strong external magnetic field especially for high-frequency applications. These external fields come from a permanent magnet which provides fields in the order of 10s of Oe or by the Oersted field created by a current through a loop where larger currents are required for larger fields which also require a cooling system. With undulating CoFeB, high-frequency oscillations can be excited at low fields thus enabling the realization of miniaturized, light weight, and portable microwave components in the K-band (18 to 27 GHz).

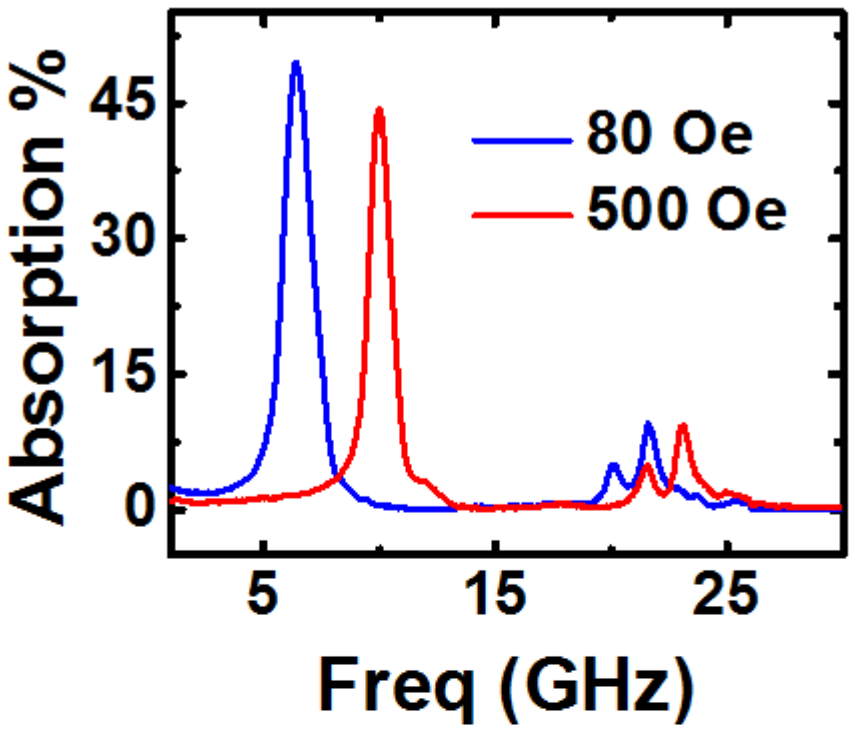
Absorption %
45
30
15
0
80 Oe
500 Oe
5
15
25
Freq (GHz)

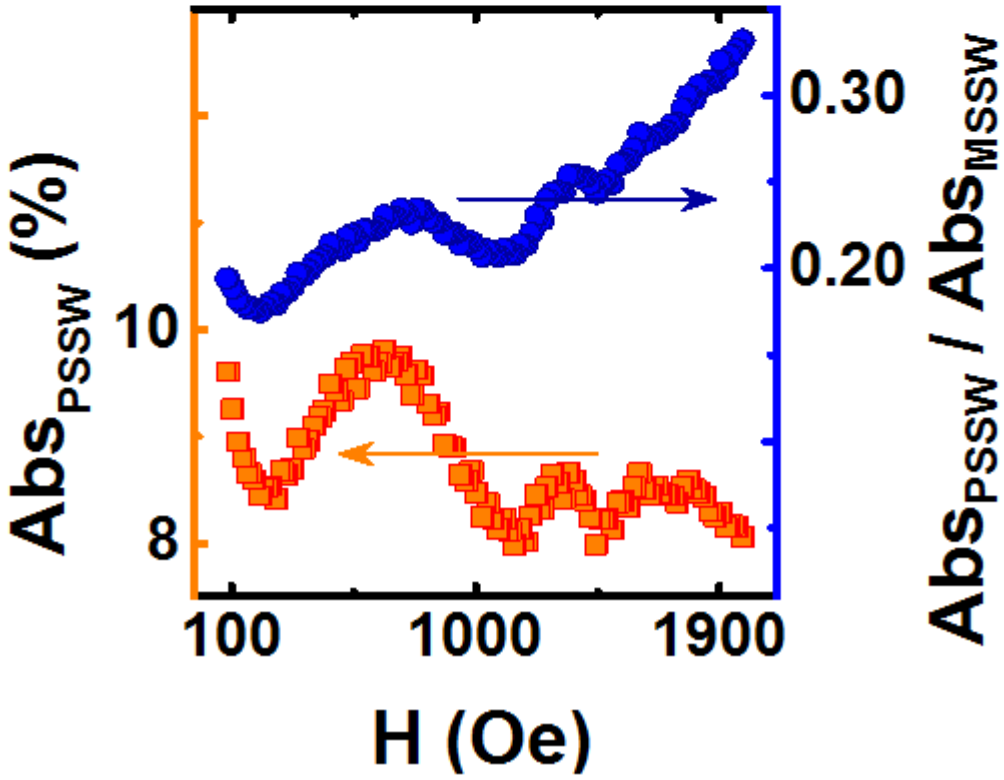
Abs$_{PSSW}$ (%)
10
8
0.30
0.20
Abs$_{PSSW}$ / Abs$_{MSSW}$
100
1000
1900
H (Oe)

Figure 6. Efficiency of PSSW excitation. a) RF power absorbed by undulating CoFeB derived from S_{11} parameters at bias fields of 80 Oe (blue dashed line) and 500 Oe (red solid line) show the absorption of MSSW and PSSW modes. b) The orange squares show the amount of RF power absorbed by the PSSW mode at bias fields ranging from 80 to 1990 Oe. The data represents the local maximum of the PSSW mode (center frequency) and shows a maximum absorption of nearly 10% at bias fields below 100 Oe. Relative excitation efficiency, shown by blue circles, is defined as the ratio of the peak power absorbed by at the PSSW center frequency normalized by the peak power absorbed at the MSSW center frequency. The CoFeB layer shows excitation efficiency of 20% at low bias fields.

VII. CONCLUSIONS

In summary, we have demonstrated that high-frequency magnetic oscillations can be efficiently excited at low fields (even below 100 Oe) in the form of PSSW in undulating CoFeB films. Using the periodically undulating silicon oxide substrate that we have fabricated, other FM materials can also be used and studied. PSSW modes have mostly been used for determining FM material parameters such as exchange stiffness whereas other spin-wave modes have been utilized in other practical applications as well. With the possibility of efficient excitation of high-frequency exchange-dominated modes such as PSSW, new possibilities in spintronic applications are now feasible.

VIII. ACKNOWLEDGMENTS

This work was supported in part by the NSF engineering research center on translational applications of nanoscale multiferroic systems (TANMS) and King Abdulaziz City for Science and Technology (KACST). We would also like to thank Prof. Andrei Slavin for his contribution to the theoretical understanding of the experimental observations. The fabrication of the devices was done at Nanoelectronics Research Facility and the Integrated Systems Nanofabrication Cleanroom (ISNC) at the

University of California Los Angeles. We would also like to thank Farbod Ebrahimi and J. Devin Schneider for their contribution in this work.

IX. REFERENCES

[1] C. Kittel, Introduction to Solid State Physics, *Introduction to Solid State Physics*, 8th Edn (Wiley, 2005).

[2] S. O. Demokritov, B. Hillebrands, and A. N. Slavin, Brillouin Light Scattering Studies of Confined Spin Waves: Linear and Nonlinear Confinement, Phys. Rep. **348**, 441 (2001).

[3] T. Schneider, A. A. Serga, B. Leven, B. Hillebrands, R. L. Stamps, and M. P. Kostylev, Realization of Spin-Wave Logic Gates, Appl. Phys. Lett. **92**, 22505 (2008).

[4] A. Khitun, M. Bao, and K. L. Wang, Spin Wave Magnetic Nanofabric: A New Approach to Spin-Based Logic Circuitry, IEEE Trans. Magn. **44**, 2141 (2008).

[5] M. Jamali, J. H. Kwon, S.-M. Seo, K.-J. Lee, and H. Yang, Spin Wave Nonreciprocity for Logic Device Applications., Sci. Rep. **3**, 3160 (2013).

[6] A. Khitun and K. L. Wang, Nano Scale Computational Architectures with Spin Wave Bus, Superlattices Microstruct. **38**, 184 (2005).

[7] A. V. Chumak, V. I. I. Vasyuchka, A. A. A. Serga, and B. Hillebrands, Magnon Spintronics, Nat. Phys. **11**, 453 (2015).

[8] D. D. Stancil and A. Prabnakar, Spin Waves, *Spin Waves* (Springer, New York, NY, 2009).

[9] B. K. Kuanr, A. V. Kuanr, T. Fal, R. E. Camley, and Z. Celinski, Ultrathin Magnetic Multilayer Films for Low-Field Microwave Notch Filters, J. Vac. Sci. Technol. B Microelectron. Nanom. Struct. **25**, 2603 (2007).

[10] I. S. Maksymov and M. Kostylev, Broadband Stripline Ferromagnetic Resonance Spectroscopy of

Ferromagnetic Films, Multilayers and Nanostructures, Phys. E Low-Dimensional Syst. Nanostructures **69**, 253 (2015).

[11] A. Haldar, C. Banerjee, P. Laha, and A. Barman, Brillouin Light Scattering Study of Spin Waves in NiFe/Co Exchange Spring Bilayer Films, J. Appl. Phys. **115**, 133901 (2014).

[12] H. S. Song, K. D. Lee, C. Y. You, S. H. Yang, S. Parkin, B. G. Park, J. W. Sohn, J. Il Hong, and S. C. Shin, Intrinsic and Extrinsic Gilbert Damping in Exchange-Biased IrMn/Cu/CoFe Trilayer Films, Appl. Phys. Express **8**, 53002 (2015).

[13] A. Conca, E. T. Papaioannou, S. Klingler, J. Greser, T. Sebastian, B. Leven, J. L??sch, and B. Hillebrands, Annealing Influence on the Gilbert Damping Parameter and the Exchange Constant of CoFeB Thin Films, Appl. Phys. Lett. **104**, 182407 (2014).

[14] S. Klingler, a V Chumak, T. Mewes, B. Khodadadi, C. Mewes, C. Dubs, O. Surzhenko, B. Hillebrands, and a Conca, Measurements of the Exchange Stiffness of YIG Films Using Broadband Ferromagnetic Resonance Techniques, J. Phys. D. Appl. Phys. **48**, 15001 (2015).

[15] C. Bilzer, T. Devolder, J.-V. Kim, G. Counil, C. Chappert, S. Cardoso, and P. P. Freitas, Study of the Dynamic Magnetic Properties of Soft CoFeB Films, J. Appl. Phys. **100**, 53903 (2006).

[16] M. A. W. Schoen, J. M. Shaw, H. T. Nembach, M. Weiler, and T. J. Silva, Radiative Damping in Waveguide-Based Ferromagnetic Resonance Measured via Analysis of Perpendicular Standing Spin Waves in Sputtered Permalloy Films, Phys. Rev. B - Condens. Matter Mater. Phys. **92**, 184417 (2015).

[17] T. Seki, K. Utsumiya, Y. Nozaki, H. Imamura, and K. Takanashi, Spin Wave-Assisted Reduction in Switching Field of Highly Coercive Iron-Platinum Magnets., Nat. Commun. **4**, 1726 (2013).

[18] F. Busse, M. Mansurova, B. Lenk, M. von der Ehe, and M. Münzenberg, A Scenario for Magnonic Spin-Wave Traps, Sci. Rep. **5**, 12824 (2015).

[19] B. Lenk, G. Eilers, J. Hamrle, and M. Münzenberg, Spin-Wave Population in Nickel after Femtosecond Laser Pulse Excitation, Phys. Rev. B - Condens. Matter Mater. Phys. **82**, 134443 (2010).

[20] Y. Ding, T. J. Klemmer, and T. M. Crawford, A Coplanar Waveguide Permeameter for Studying High-Frequency Properties of Soft Magnetic Materials, J. Appl. Phys. **96**, 2969 (2004).

[21] D. I. Mircea and T. W. Clinton, Near-Field Microwave Probe for Local Ferromagnetic Resonance Characterization, Appl. Phys. Lett. **90**, 142504 (2007).

[22] See Supplemental Material at [URL Will Be Inserted by AIP] for detailed fabrications steps, YIG sample preparation, and simulation details., (n.d.).

[23] H. Seidel, L. Csepregi, a. Heuberger, and H. Baumgärtel, Anisotropic Etching of Crystalline Silicon in Alkaline Solutions, J. Electrochem. Soc. **137**, 3612 (1990).

[24] M. Bailleul, D. Olligs, C. Fermon, and S. O. Demokritov, Spin Waves Propagation and Confinement in Conducting Films at the Micrometer Scale, Europhys. Lett. **56**, 741 (2001).

[25] M. Bao, K. Wong, A. Khitun, J. Lee, Z. Hao, K. L. Wang, D. W. Lee, and S. X. Wang, Determining Wave Vector and Material Property from the Phase-Shift of Spin-Wave Propagation, EPL (Europhysics Lett. **84**, 27009 (2008).

[26] V. Vlaminck and M. Bailleul, Spin-Wave Transduction at the Submicrometer Scale: Experiment and Modeling, Phys. Rev. B - Condens. Matter Mater. Phys. **81**, 14425 (2010).

[27] J. H. Kwon, S. S. Mukherjee, P. Deorani, M. Hayashi, and H. Yang, Characterization of Magnetostatic Surface Spin Waves in Magnetic Thin Films: Evaluation for Microelectronic Applications, Appl. Phys. A Mater. Sci. Process. **111**, 369 (2013).

[28] Y. S. Gui, N. Mecking, and C. M. Hu, Quantized Spin Excitations in a Ferromagnetic Microstrip from Microwave Photovoltage Measurements, Phys. Rev. Lett. **98**, 217603 (2007).

[29] B. A. Kalinikos and A. N. Slavin, Ferromagnetic Films With Mixed Exchange Boundary, J. Phys. C Solid State Phys. **19**, 7013 (1986).

[30] Y. Sun, Y. Y. Song, H. Chang, M. Kabatek, M. Jantz, W. Schneider, M. Wu, H. Schultheiss, and A. Hoffmann, Growth and Ferromagnetic Resonance Properties of Nanometer-Thick Yttrium Iron Garnet Films, Appl. Phys. Lett. **101**, 152405 (2012).

[31] A. Vansteenkiste and B. Van De Wiele, MUMAX: A New High-Performance Micromagnetic Simulation Tool, J. Magn. Magn. Mater. **323**, 2585 (2011).

[32] G. S. Abo, Y. Hong, J. Park, J. Lee, W. Lee, and B. Choi, Definition of Magnetic Exchange Length, **49**, 4937 (2013).

[33] I. Barsukov, P. Landeros, R. Meckenstock, J. Lindner, D. Spoddig, Z. A. Li, B. Krumme, H. Wende, D. L. Mills, and M. Farle, Tuning Magnetic Relaxation by Oblique Deposition, Phys. Rev. B - Condens. Matter Mater. Phys. **85**, 14420 (2012).